Optimizing the Frangi Filter: SCALR – A Machine Learning Model for Scale Prediction in Perivascular Space Quantification

Juan S. Diaz Villota[a], Maria Trujillo[a], Jose Bernal[a,b,c,d,e]

[a]*Multimedia and Computer Vision Group, Universidad del Valle, Calle 13 No. 100-00, Cali, 760032, Valle del Cauca, Colombia*
[b]*German Centre for Neurodegenerative Diseases (DZNE), Leipziger Str. 44, Magdeburg, 39120, Germany*
[c]*Institute of Cognitive Neurology and Dementia Research, Otto-Von-Guericke University Magdeburg, Leipziger Str. 44, Magdeburg, 39120, Germany*
[d]*Centre for Clinical Brain Science, The University of Edinburgh, 49 Little France Crescent, Edinburgh, EH16 4SB, UK*
[e]*UK Dementia Research Institute Centre at the University of Edinburgh, Edinburgh Bioquarter, 49 Little France Crescent, Edinburgh, EH16 4SB, UK*

Abstract

Growing interest in perivascular spaces (PVS) quantification has highlighted the need for accurate and robust methods, particularly in magnetic resonance imaging (MRI). The Frangi filter is widely used to enhance tubular structures, including PVS, however its performance is highly dependent on scale selection. In the context of computer vision, "scale" refers to the size of the structures or features being detected by a filter or detector. In multiscale filtering, multiple scales are used to capture structures of varying sizes, and an optimal scale corresponds to the size at which a structure of interest is best enhanced or detected. Despite advancements in multiscale filtering techniques, determining an optimal scale for PVS quantification remains an open challenge.

We introduce SCALR, a machine learning-based approach for scale selection in Frangi filtering to improve PVS quantification. A linear regression model, trained on synthetic and real MRI data, is used to infer an optimal scale based on a range of noise levels and voxel sizes across various imaging conditions. The findings indicate that SCALR enhances PVS detection, particularly in low signal-to-noise ratio MRI. By automating scale selection, SCALR increases the reliability of quantification and provides a scalable solution for integrating Frangi-based PVS analysis into clinical and research workflows.

Keywords: Perivascular spaces, Cerebral small vessel disease, Frangi filter, Scale-space theory, Image processing, Machine learning

Abbreviations

MRI, Magnetic resonance imaging; PVS, Perivascular spaces; ROI, Region of interest; SNR, Signal-to-noise ratio; CSO, Centrum semiovale; BG, Basal ganglia

1. Introduction

Perivascular Spaces (PVS) are small, fluid-filled tubular structures typically measuring less than 2 millimeters in diameter. They surround cerebral arterioles and venules and are predominantly found in regions such as the basal ganglia (BG), centrum semiovale (CSO), and midbrain. PVS are hypothesised to play a crucial role in the brain's glymphatic system, which is responsible for clearing waste products from the central nervous system. Specifically, PVS are thought to act as drainage channels that facilitate the elimination of proteins, metabolic waste, and toxic metabolites (1). This function underscores their potential significance in maintaining brain health and homeostasis.

Although PVS are naturally present in all brains, they are typically not visible on MRIs unless they become enlarged, a condition known as enlarged perivascular spaces (ePVS). The enlargement of these spaces is associated with aging, neurodegenerative diseases, and trauma. In particular, ePVS have been identified as potential biomarkers for impaired clearance within the central nervous system, with their presence hypothesised to be linked to several neurological conditions, including Alzheimer's and Parkinson's diseases (15), small vessel disease, and other neurodegenerative disorders (2). Consequently, the study of ePVS presence and distribution in MRI scans has gained increasing attention, with important implications for understanding brain health and disease progression (24).

Accurate PVS quantification is essential for assessing small vessel disease and other neurological disorders. Various computational methods have been developed for this task, primarily falling into two categories: deterministic approaches, such as the Hessian-based Frangi filter (6; 23), and statistical models, notably convolutional neural networks (CNNs) (11). While CNNs can achieve high segmentation accuracy, their effectiveness depends on large annotated datasets, which are often scarce in medical imaging. Additionally, CNNs function as '"black-box" models, limiting interpretability (12). In contrast, deterministic methods like the Frangi filter offer mathematical transparency and remain widely used due to their effectiveness in enhancing small tubular structures (27).

The performance of the Frangi filter is highly dependent on parameter selection, particularly the scale parameter, which determines sensitivity to structure size (see Figure 1). Manually tuning this parameter is time-consuming and prone to inconsis-

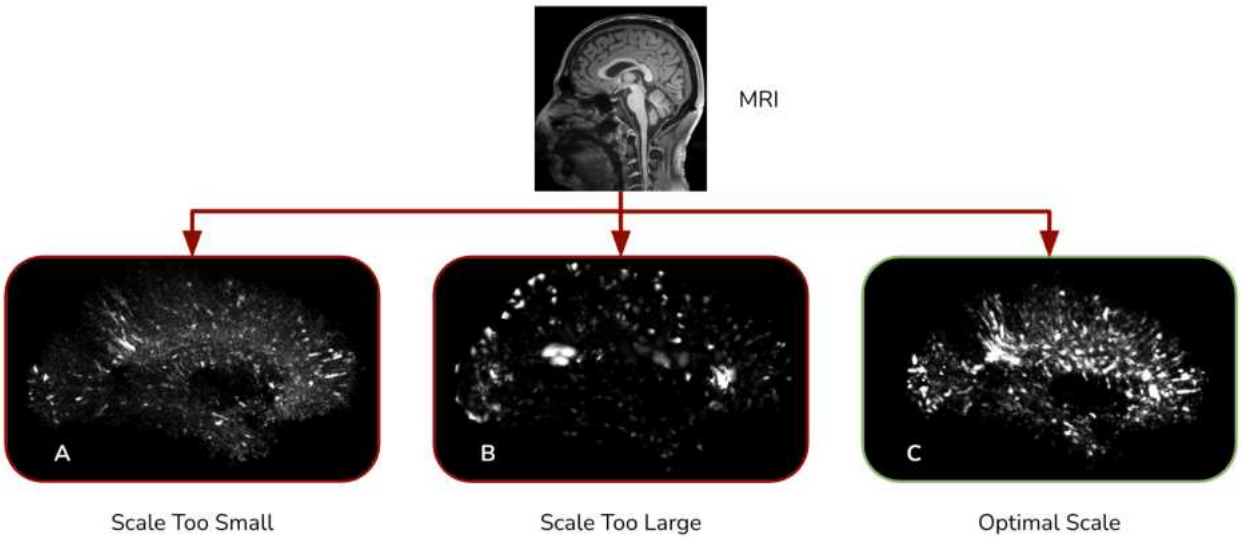

Figure 1: Comparison of the output of the Frangi filter at different scales. (A) PVS output at a very small scale, where PVS are visible, but significant noise is present. (B) Output at a large scale, where noise is reduced, but important features are discarded. (C) Output at an optimal scale, where PVS remain visible while minimizing noise.

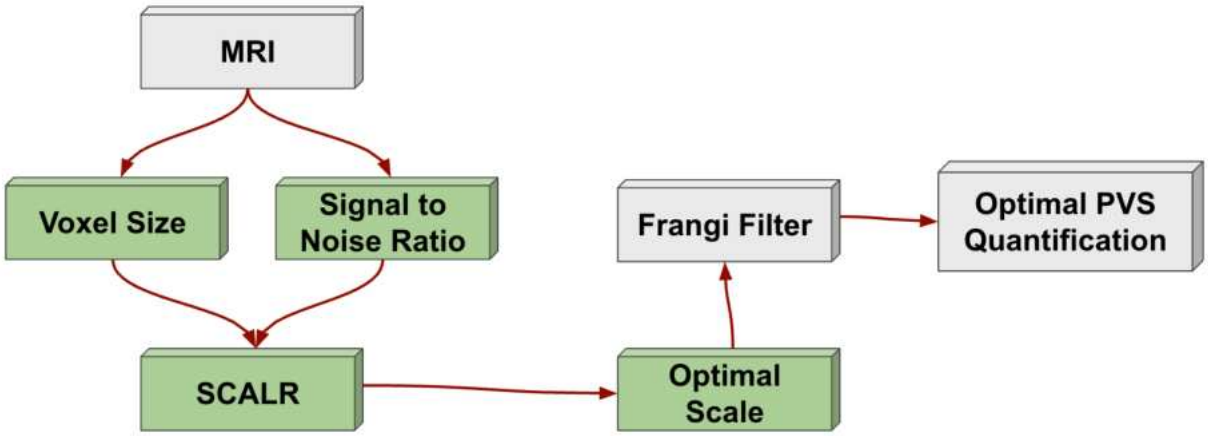

Figure 2: SCALR diagram illustrating the process of determining an optimal scale for improved PVS quantification.

tency, especially across heterogeneous datasets. Despite various efforts to improve PVS segmentation, the Frangi filter remains one of the most effective Hessian-based multiscale methods, provided that optimal parameters are selected and MRI quality is sufficient (3).

Typically, the scale parameter is set by a specialist, technician, or software developer using default values optimised for the average MRI scan. However, these values do not account for variations in imaging conditions, leading to inconsistent segmentation performance. Some MRIs benefit from well-matched parameters, while others suffer from suboptimal selection. The absence of a systematic approach for determining the optimal scale for each image reduces the reliability of the Frangi filter in both clinical and research applications.

To address this limitation, SCALR, a linear regression model, was developed to predict an optimal scale for the Frangi filter based on imaging conditions. SCALR leverages key MRI characteristics, including noise levels and voxel resolution, to determine an optimal scale for PVS detection (see Figure 2). The model was trained under varying acquisition conditions and noise levels, ensuring broad applicability.

Results indicate that SCALR significantly improves detection accuracy, particularly in low-SNR settings where conventional parameter tuning methods often fail. By reliably predicting an optimal scale, SCALR reduces the need for trial-and-error adjustments, streamlining the PVS quantification process. This approach not only minimises processing time but also enables the optimisation of additional filter parameters, enhancing

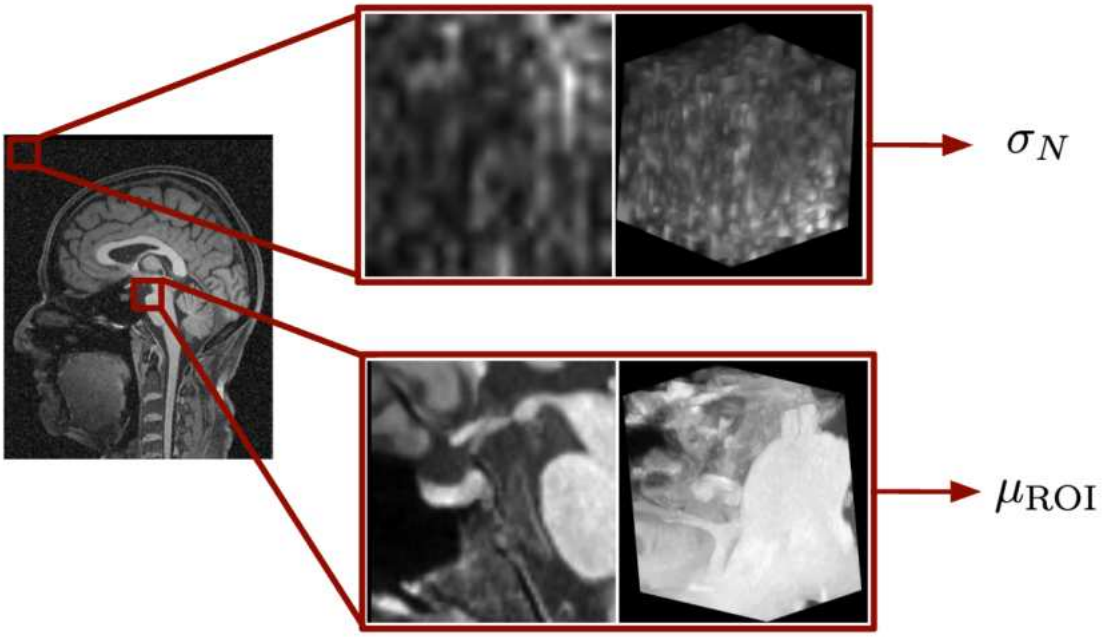

Figure 3: Illustration of SNR measurement: The standard deviation of noise (σ_N) is calculated from the corners of the image, while the mean signal intensity (μ_{ROI}) is computed from a central region containing the tissue signal.

overall PVS analysis. SCALR represents a promising advancement in automated PVS detection, providing an efficient and precise method for both researchers and clinicians (28).

2. Materials & Methods

The SCALR model aims to determine an optimal scale based on the quality of an MRI scan. Higher-quality images enhance PVS visibility; however, in lower-quality MRIs, two primary factors significantly impact PVS detection: noise level and image resolution.

2.1. Measuring the SNR

SCALR estimates an optimal scale by evaluating both the SNR and the voxel size of the image. The voxel size can be directly retrieved from image metadata, providing a straightforward measure of resolution. However, noise quantification is more complex and requires additional processing steps.

The SNR quantifies the proportion of noise relative to a signal and is defined as:

$$\text{SNR} = \frac{\mu_{\text{ROI}}}{\sigma_N} \tag{1}$$

where μ_{ROI} represents the mean signal intensity within a selected region of interest (ROI), and σ_N denotes the standard deviation of the noise. It should be noted that equation 1 follows an exponential decay. SNR approaches infinity when no noise is present ($\sigma_N = 0$), and tend towards 1 as the noise and the signal reach the same average intensity ($\sigma_N \approx \mu_{\text{ROI}}$).

To estimate σ_N in an MRI scan, the standard deviation of voxel intensities is computed in a homogeneous volume assumed to contain only noise. This volume is selected from the corners of the image, where no anatomical structures are present, ensuring a dark background with minimal signal contribution.

The value of μ_{ROI} is obtained from a central region covering 15% of the image volume, as this location consistently contains tissue in MRI scans (see Figure 3). This measurement is used to find an optimal scale across different MRI configurations with varying levels of quality.

2.2. SCALR Model

The model was built using a dataset consisting of 318 images, reshaped to ensure isotropic voxels across all samples for consistency. The dataset comprises three distinct groups, each used to train the model under different quality scenarios:

2.2.1. Real Denoised Images

The first group consists of real denoised images (7) with a voxel size of 0.8 mm, collected from 15 subjects. Each subject contributed a set of images that represent various anatomical structures. Corresponding PVS masks, manually annotated by professional experts, were used to accurately identify PVS in the brain (see Figure 4).

2.2.2. Hybrid Images

The second group comprises hybrid images derived from the 15 real images. These underwent downsampling to produce resolutions ranging from 0.8 mm to 1.5 mm voxel size. Rician noise was introduced to simulate varying noise environments commonly encountered in MRI scans, resulting in 198 hybrid images. This group was designed to help the model learn to distinguish between signal and noise, thus improving its robustness to noise in real-world scenarios (see Figure 5).

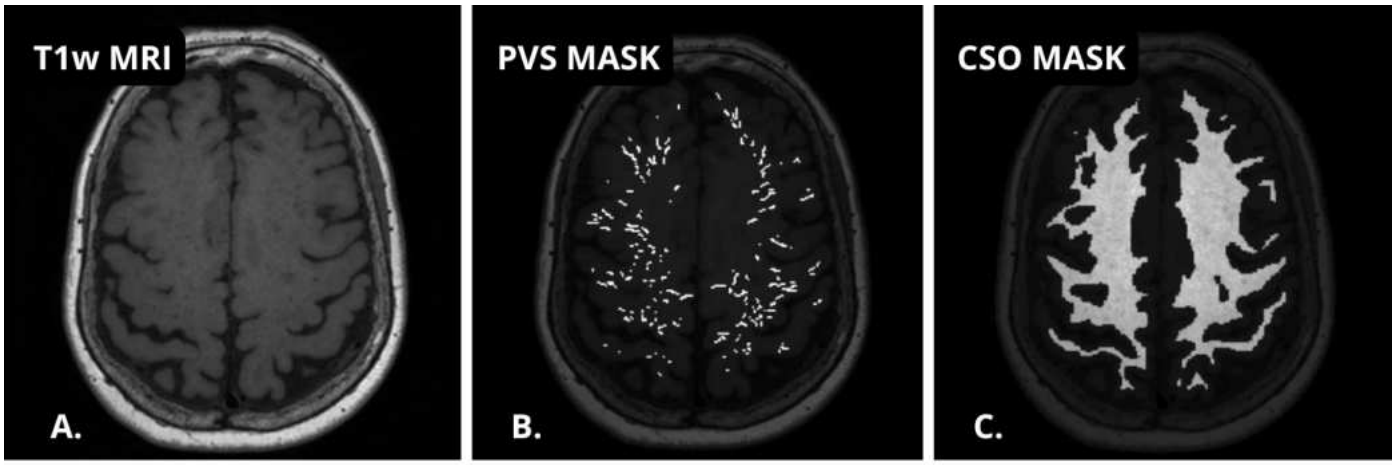

Figure 4: MRI sample from the real denoised MRI dataset. (A) T1w MRI. (B) PVS mask. (C) CSO mask.

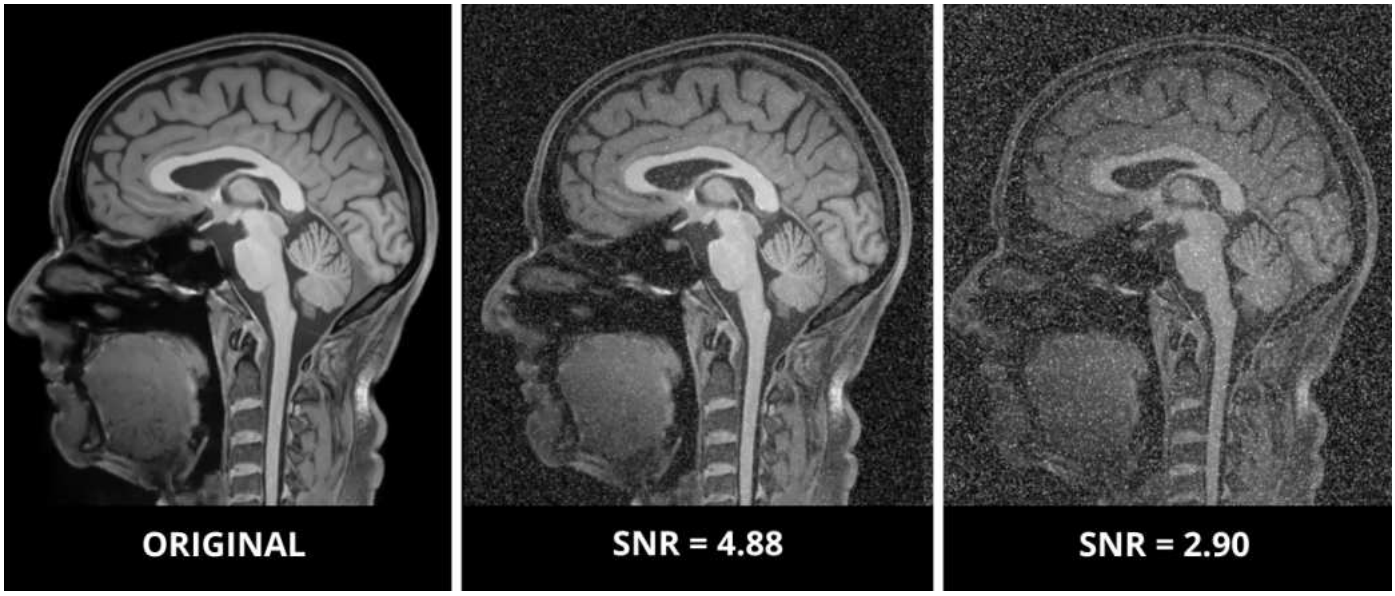

Figure 5: MRI sample from the hybrid dataset, generated by resampling real images and adding noise.

2.2.3. Synthetic Images

The third group consists of 105 synthetic images with a voxel size of 1 mm and their corresponding PVS masks, generated using the PVS-DRO generator developed by Jose Bernal (20). These images were specifically designed to simulate PVS patterns in a controlled environment, representing subjects from various age groups, ranging from 25 to 92 years old. The dataset includes MRI scans in T1-weighted (T1w), T2-weighted (T2w), and FLAIR sequences (see Figure 6); however, only T1w images were used for training.

2.3. Determining an optimal Scale

In the process of training the model, it is crucial to establish a method for selecting an optimal scale. The optimal scale, as proposed in this paper, is defined as the scale that maximises the contrast between the PVS and the surrounding area.

To quantify this contrast, the PVS mask was treated as the region of interest (ROI), while a boundary shell surrounding the mask was designated as the contrasting region (see Figure 7). This approach allowed for an evaluation of the scale's effectiveness in enhancing the visibility of the PVS. The scale that produced the highest contrast between the PVS and the surrounding area is selected as an optimal scale for further processing.

For each image in the dataset, scales from 0 to 2.5 mm were applied. Voxel size was considered to standardise measurements in millimeters. At each scale, PVS mask contrast was calculated, and the scale yielding the highest contrast was selected as optimal (see Figure 8).

The optimal scale for each MRI was then stored (Table 1) and mapped to analyze trends across voxel sizes and SNR values (see Figure 9).

It is important to note that, although noise exhibits random

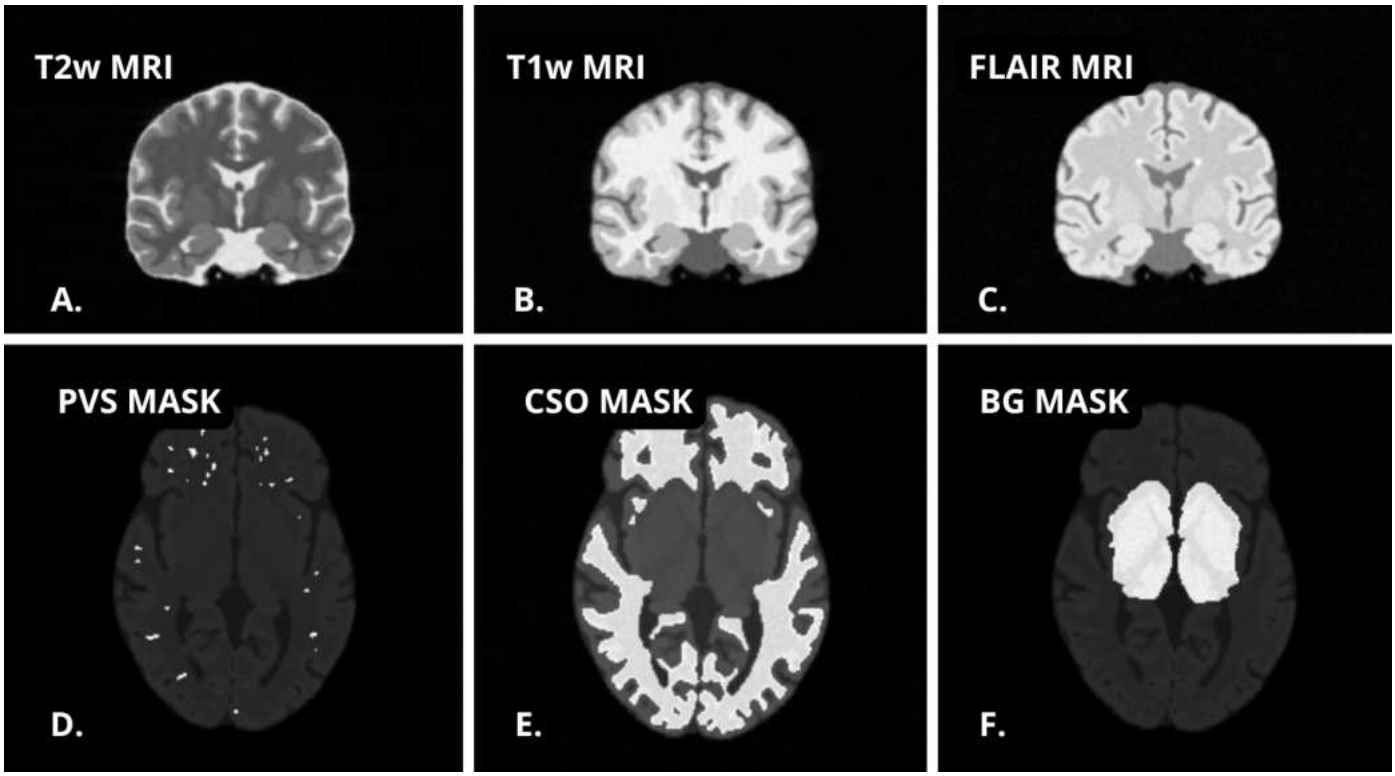

Figure 6: Brain samples from the synthetic MRI dataset generated using the PVS-DRO framework by José Bernal. The top row shows MRI modalities: (A) T2-weighted, (B) T1-weighted, and (C) FLAIR. The bottom row displays the corresponding masks provided by the generator: (D) PVS mask, (E) CSO mask, and (F) BG mask.

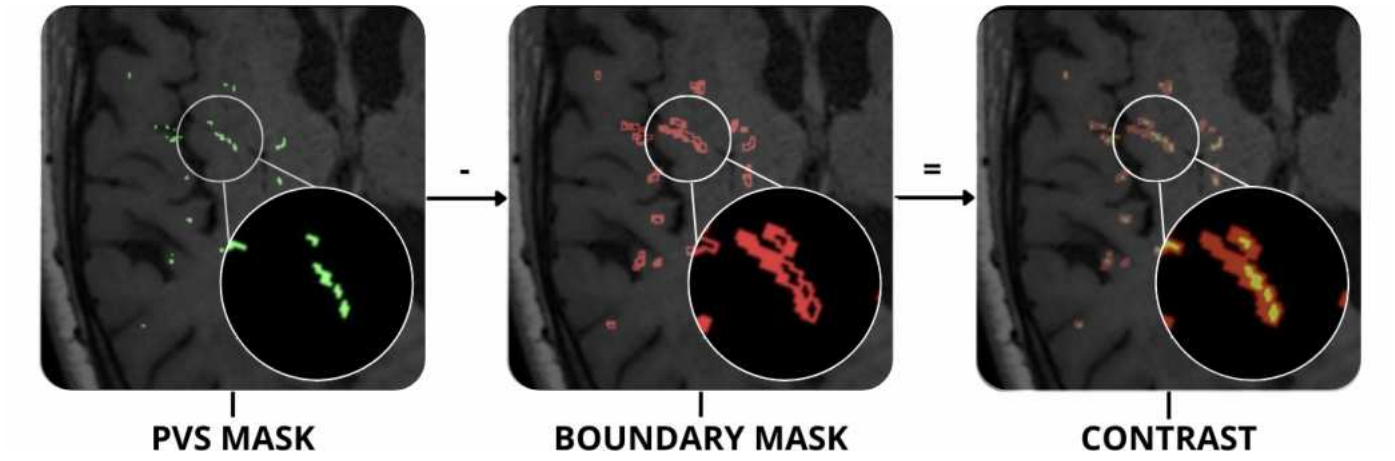

Figure 7: Slice of the PVS mask (green) and boundary mask (red) with a 1 mm thickness, used to measure PVS contrast across different scales. MRI sample from Figure 4.

behavior, this randomness generally follows a smooth trajectory that the model can leverage to make reliable predictions.

Consider, for instance, the MRI sample from the hybrid dataset shown in Figure 5 with varying levels of noise applied. As additional noise is introduced into the image, the optimal scale shifts (see Figure 10). Although the exact behavior of this shift remains uncertain, interpolation methods can approximate a trend that aligns with the majority of the data points.

Higher-degree polynomials were found to tend to overfit the data, capturing the randomness of the variations in data rather than the underlying trend. On the other hand, lower-degree polynomials may fail to capture the data's complexity, leading to underfitting.

The model is trained and tested using the same dataset by splitting it into two groups: one for training and the other for testing. The performance of each model was evaluated using

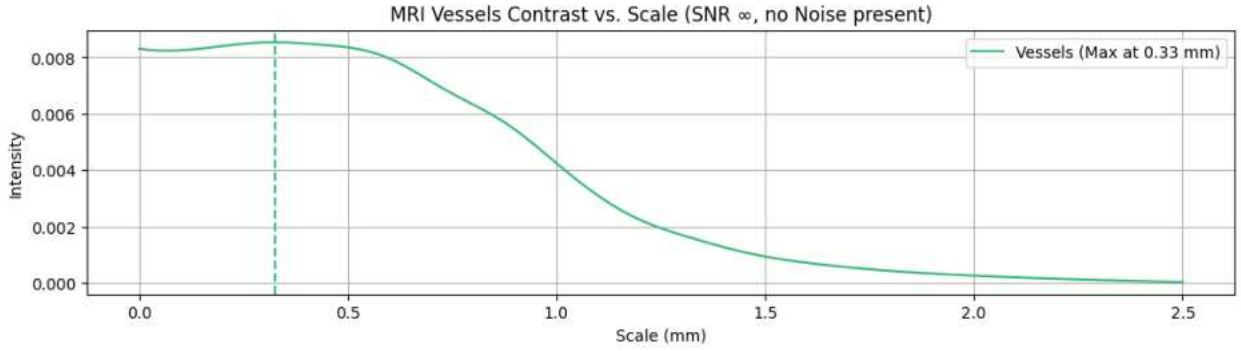

Figure 8: Plot depicting the average contrast of the vessels in the MRI sample from Figure 7, highlighting the scale at which maximum intensity is achieved (scales ranging from 0 to 2.5 millimetres).

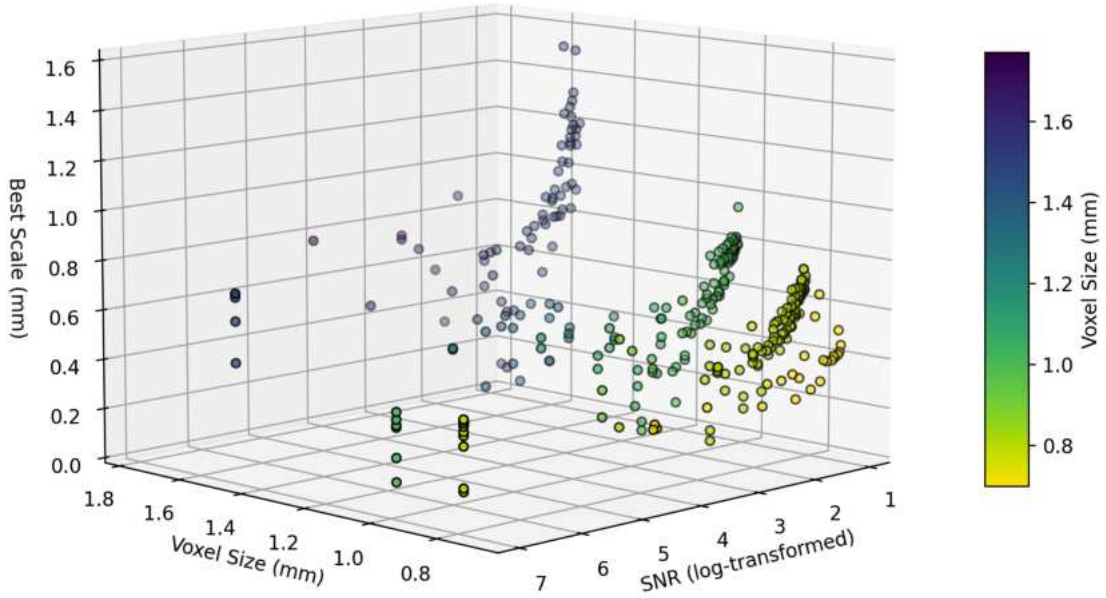

Figure 9: 3D plot of points from table 1 representing the measurements of each image in the dataset. The x-axis corresponds to the noise level (SNR), the y-axis represents the image resolution (voxel size), and the z-axis indicates the measured optimal scale. High-resolution images are depicted in yellow, low-resolution images are shown in blue.

ID	SNR	Voxel Size (mm)	Optimal Scale (mm)
94	2.354789	0.80	0.621118
196	2.092076	0.80	0.744147
298	42.471551	1.68	0.803577
112	4.294113	1.00	0.602007
280	26.646066	1.01	0.470497
105	2.354789	0.80	0.622074
...	...	...	...

Table 1: Summary of MRI image data, including SNR, voxel size, and optimal scale.

Mean Squared Error (MSE) and R-squared (R^2) metrics to assess the accuracy and goodness of fit.

The Mean Squared Error (MSE) is a commonly used metric that measures the average of the squared differences between the predicted and actual values. It provides a clear indication of how well the model's predictions align with the true data points, where a lower MSE indicates better predictive performance (see Table 2). MSE penalises larger errors more heavily, making it particularly useful for identifying models that may produce large deviations from the actual data.

MSE	Polynomial Degree			
Test Size	2	3	4	5
10%	0.0203	0.0151	0.0132	0.0135
20%	0.0209	0.0128	0.0126	0.0135
30%	0.0257	0.0152	0.0217	0.0573
40%	0.0212	0.0150	0.0210	0.0685
50%	0.0202	0.0148	0.0206	0.0547

Table 2: Mean Squared Error (MSE) for Different Degrees and Test Sizes with Heatmap Coloring, where darker tones indicate better scores.

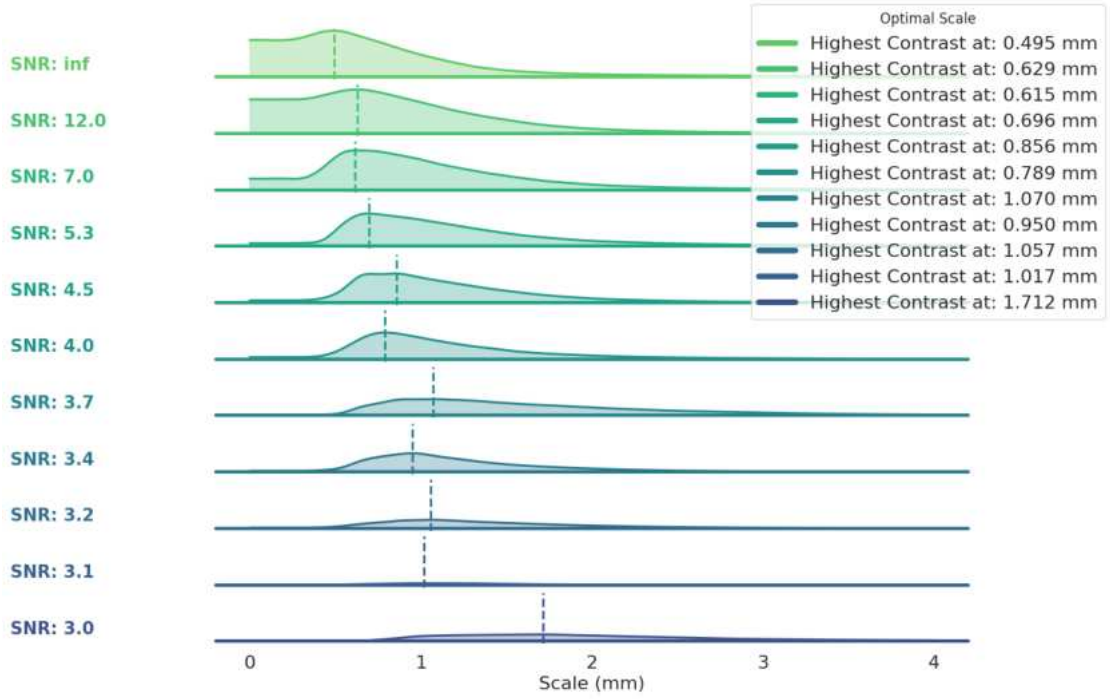

Figure 10: Plot illustrating the shift in the optimal scale as the noise level increases, based on the sample MRI shown in Figure 5.

The R-squared (R^2) metric, on the other hand, measures the proportion of the variance in the dependent variable that is predictable from the independent variables. An R^2 value close to 1 indicates that a model explains most of the variance in the data, while a value closer to 0 suggests poor predictive power (see Table 3).

R^2	Polynomial Degree			
Test Size	2	3	4	5
10%	0.7187	0.7903	0.8163	0.8119
20%	0.6782	0.8035	0.8061	0.7915
30%	0.5965	0.7615	0.6595	0.1024
40%	0.6728	0.7681	0.6760	-0.0530
50%	0.6817	0.7671	0.6765	0.1412

Table 3: R^2 Score for Different Degrees and Test Sizes, where darker tones indicate better scores closer to 1. Lower values have less color.

Together, MSE and R^2 provide complementary insights into the model's performance: MSE focuses on prediction error, while R^2 highlights the overall explanatory power (10). After testing various combinations of polynomial degrees and test sizes, an optimal configuration was determined to be a third-degree polynomial with a 20% test size. The performance metrics of the model are summarised in Table 4. This configuration offers the best balance between model complexity and predictive performance, as higher-degree polynomials increase the risk of overfitting while providing limited improvement in model accuracy.

SCALR model can be visualised as a polynomial surface that illustrates the relation among SNR, voxel size, and predicted optimal scale. Figure 11 provides a detailed view of the model's response surface, clarifying how scale predictions are adjusted in response to image quality parameters.

Metric	Value
Mean Squared Error (MSE)	0.0128
R^2 Score	0.8035

Table 4: SCALR Model Evaluation on the best configuration

3. Results

SCALR was evaluated on MRI scans that were not included in the dataset, the model produces predictions that closely align with the measured optimal scale for the image determined using the method described in Section 2.3. This indicates the precision of SCALR in identifying an optimal scale for segmentation.

ID	SNR	Voxel Size	Best Scale	SCALR
1	1.601631	1.00	0.759	0.765
2	11.018970	1.01	0.470	0.433
3	3.741848	1.50	0.476	0.666
4	17.045681	0.84	0.395	0.413
5	14.627818	0.80	0.627	0.592

Table 5: SCALR model predictions. Darker shades indicate closer values between the best scale and the predicted scale.

For instance, consider the last subject in Table 5 (ID 5). By evaluating scales adjacent to the SCALR prediction—one be-

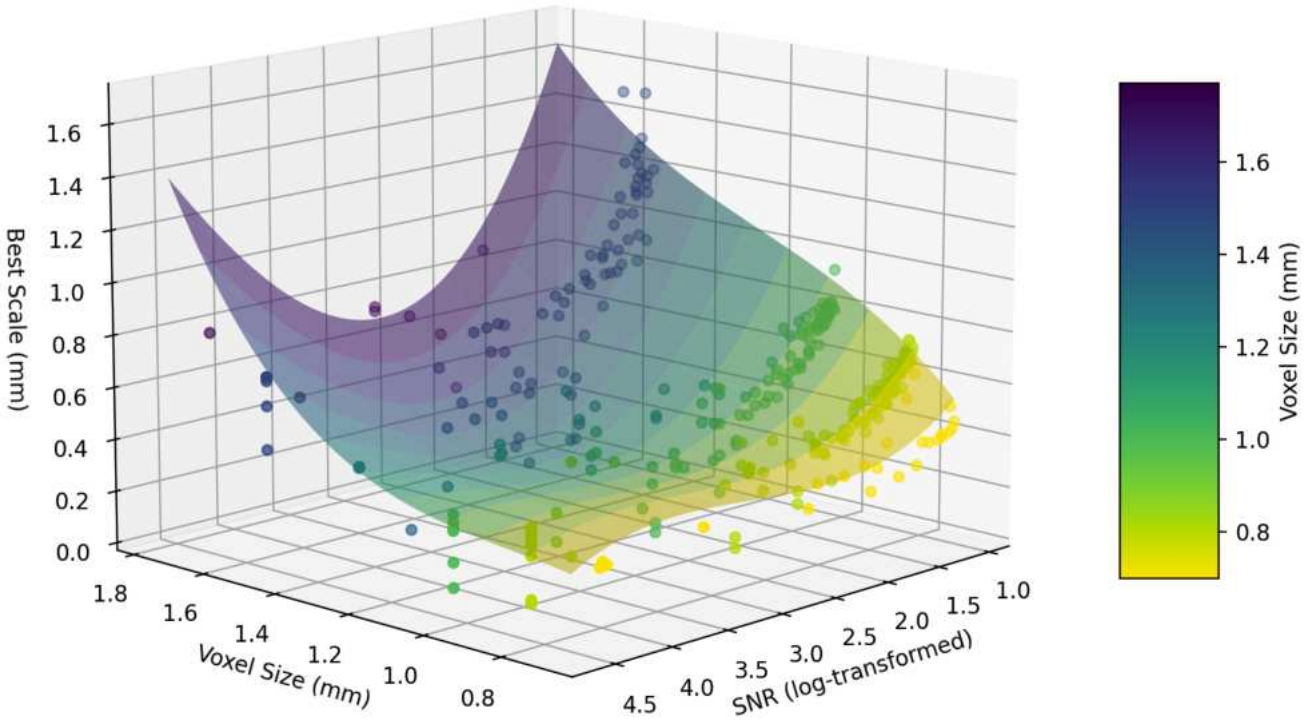

Figure 11: 3D surface plot of the SCALR model. This visualisation illustrates the best interpolation for the data shown in Figure 9, showing how the SCALR model dynamically adjusts scale predictions in response to image quality parameters.

low and one above—it becomes clear that a smaller scale introduces noise, while a larger scale distorts the PVS morphology. Figure 12 presents a comparative volume rendering of the segmented PVS from the MRI processed at different scales. The middle image (labelled B) corresponds to the scale predicted by SCALR, where the PVS structures are clearly visible with minimal noise and high detail. In contrast, subfigure A (smaller scale) introduces significant noise, complicating segmentation, while subfigure C (larger scale) reduces noise but distorts the PVS, obscuring crucial details. This comparison underscores the SCALR model's ability to select an optimal scale for accurate segmentation.

4. Discussion

The Frangi filter is a well-established tool for PVS quantification in MRI scans; however, it is prone to overestimation due to its high sensitivity to noise, leading to inaccurate segmentation. SCALR mitigates this issue by inferring an optimal scale for the filter, marking a novel contribution as no prior predictive models specifically addressed this aspect. Despite being trained on a relatively small dataset, SCALR demonstrated promising performance, with its accuracy expected to improve as it is exposed to more diverse image data.

SCALR strikes a balance between interpretability and performance by refining scale selection for the Frangi filter, improving segmentation accuracy without requiring extensive training data. This approach ensures a more reliable extraction of vessel structures, particularly in images with high noise levels, where traditional methods struggle. Furthermore, SCALR's predictive framework enables adaptation to varying acquisition protocols and scanner types, enhancing its applicability across diverse datasets.

Although SCALR was developed for PVS quantification, its underlying methodology could extend to other vessel-like structures in medical imaging, such as retinal blood vessels or coronary arteries. By addressing a fundamental limitation of the Frangi filter, SCALR contributes to improving vessel segmentation across multiple domains.

5. Conclusions and Future Work

SCALR enhances Frangi filter application in MRI analysis by efficiently determining an optimal scale for vessel quantification, eliminating the need for trial-and-error approaches. This advancement streamlines diagnostic workflows, saving time and resources.

This study highlights the potential of machine learning to extract valuable patterns from image data (26), reducing both computational costs and processing time. The high R^2 value supports SCALR's predictive validity, demonstrating strong alignment with real-world data. Moreover, its computational efficiency allows for deployment across various devices without compromising performance, making it a promising tool for quantifying PVS as a biomarker for neurological conditions.

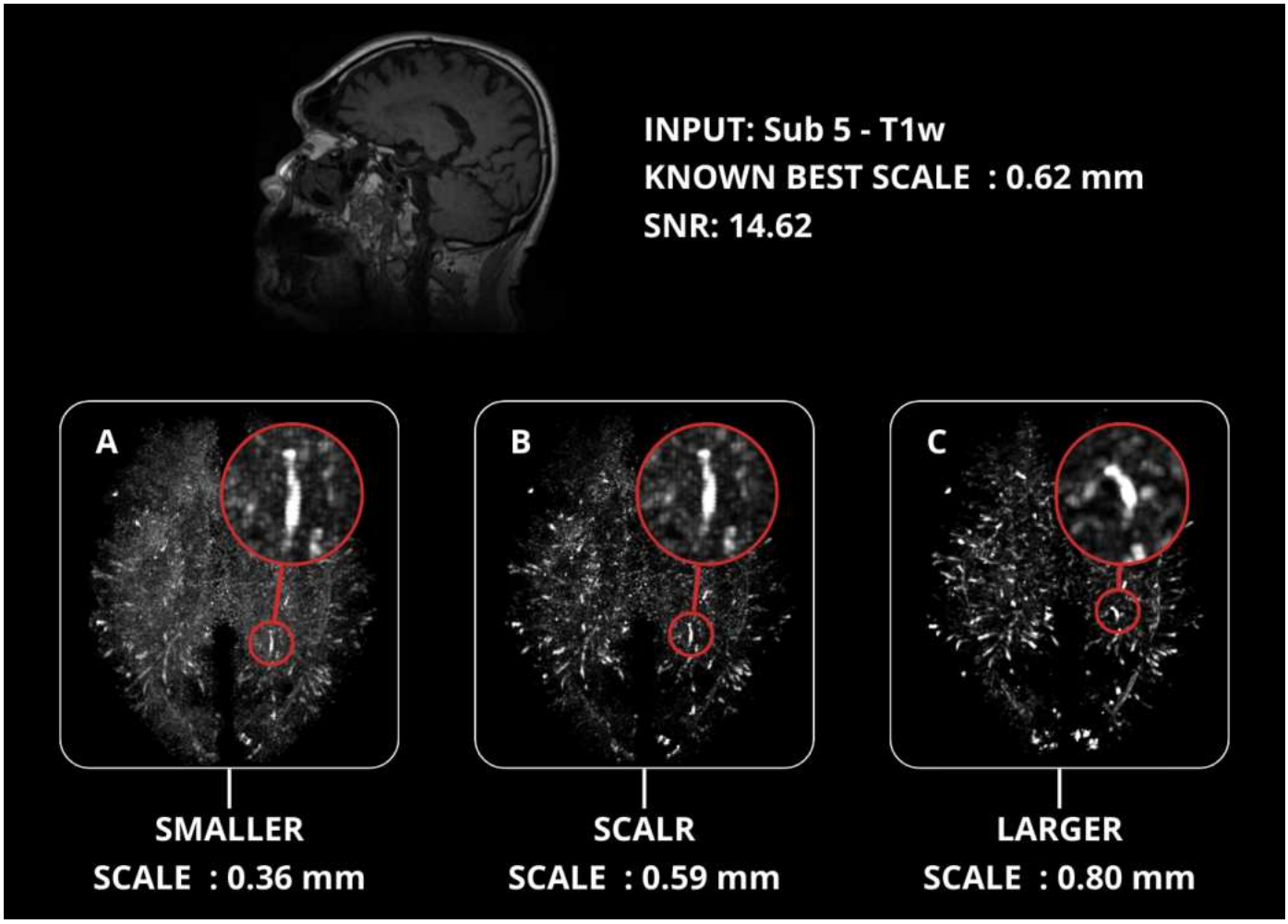

Figure 12: Volume rendering of the segmented PVS for Subject 5 from Table 5, shown at the scale recommended by SCALR (B), with additional renderings at adjacent scales (A and C) for contrast comparison.

SCALR's limitations include reduced stability with low-resolution images and reliance on a relatively small annotated dataset, which may restrict generalisability. However, MRI scans used for PVS detection typically fall within the resolution range on which SCALR was trained.

This paper establishes a reliable method for quantifying image quality via SNR and demonstrates a strong correlation between image quality and optimal scale selection. SCALR remains geometrically insightful, unlike black-box CNN models, offering transparency in its predictions. By advancing vessel detection, this work enhances the accessibility of the Frangi filter for clinical MRI analysis (13). Further validation on multi-centre datasets will be essential to ensure SCALR's robustness across different imaging protocols.

All code, including SCALR and dataset annotations, are publicly available for further research (28).

References

[1] Moses J, Sinclair B, Law M, O'Brien TJ, & Vivash L. Automated Methods for Detecting and Quantitation of Enlarged Perivascular spaces on MRI. J Magn Reson Imaging, 2023. https://doi.org/10.1002/jmri.28369.

[2] J. Ramirez, C. Berezuk, A. McNeely, G. F., J. McLaurin, & S. Black, "Imaging the perivascular space as a potential biomarker of neurovascular and neurodegenerative diseases," 2018. https://www.researchgate.net/publication/298908350_Imaging_the_Perivascular_Space_as_a_Potential_Biomarker_of_Neurovascular_and_Neurodegenerative_Diseases.

[3] Jennifer M.J. Waymont, Maria C. Valdés Hernández, Jose Bernal, Roberto Duarte Coello, Rosalind Brown, Francesca M. Chappell, Lucia Ballerini, Joanna M. Wardlaw "A Systematic Review and Meta-Analysis of Automated Methods for Quantifying Enlarged Perivascular Spaces in the Brain" medRxiv 2024. doi:https://doi.org/10.1101/2024.03.04.24303705.

[4] Chappell Potter, M. Z, & Wardlaw, "Cerebral perivascular spaces visible on magnetic resonance imaging: Development of a qualitative rating scale and its observer reliability,". 2015. doi:10.1159/000375153.

[5] Foruzan, A.H. & Zoroofi, Reza & Sato, Yoshinobu & Hori, Masatoshi. (2011). A Hessian-based filter for vascular segmentation of noisy hepatic CT scans. *International journal of computer assisted radiology and surgery. 7. 199-205.* https://doi.org/10.1007/s11548-011-0640-y.

[6] A. F. Frangi, W. J. Niessen, K. L. Vincken, & M. A. Viergever, "Multiscale vessel enhancement filtering," In *Medical Image Computing and Computer-*

Assisted Intervention – MICCAI'98, pp. 130-137, Springer, Berlin, Heidelberg, 1998. https://doi.org/10.1007/BFb0056195

[7] Debnath, Arunabha & Rai, Hari & Yadav, Chahat & Agarwal, Anjali & Bhatia, Ankit. (2013). Deblurring and Denoising of Magnetic Resonance Images using Blind Deconvolution Method. *International Journal of Computer Applications. 81. 7-12.* https://doi.org/10.5120/14046-2209.

[8] Jose Bernal, Maria D.C. Valdés-Hernández, Javier Escudero, Roberto Duarte, Lucia Ballerini, Mark E. Bastin, Ian J. Deary, Michael J. Thrippleton, Rhian M. Touyz, Joanna M. Wardlaw, 2022. Assessment of perivascular space filtering methods using a three-dimensional computational model. *Magnetic Resonance Imaging, Volume 93, 33-51* https://doi.org/10.1016/j.mri.2022.07.016.

[9] H. Adams, G. E. Brancati, D. Bos, & M. A. Ikram, "Machine learning in cerebral small vessel disease imaging: A systematic review," *NeuroImage: Clinical, 30*, 102667, 2021. https://doi.org/10.1016/j.nicl.2021.102667

[10] F. Doshi-Velez, & B. Kim, "Towards a rigorous science of interpretable machine learning," *arXiv preprint arXiv:1702.08608*, 2017.

[11] H. Chen, Q. Dou, L. Yu, J. Qin, & P. A. Heng, "Vessel enhancing techniques for MR angiography using deep learning," *Medical Image Analysis, 51*, 20-34, 2019. https://doi.org/10.1016/j.media.2018.09.008

[12] C. Rudin, "Stop explaining black box machine learning models for high-stakes decisions and use interpretable models instead," *Nature Machine Intelligence, 1*(5), 206-215, 2019. https://doi.org/10.1038/s42256-019-0048-6

[13] S. H. Park, & K. Han, "Methodologic guide for evaluating clinical performance and effect of artificial intelligence technology for medical diagnosis and prediction," *Radiology, 286*(3), 800-809, 2018. https://doi.org/10.1148/radiol.2017171920

[14] G. Litjens, T. Kooi, B. E. Bejnordi, A. A. A. Setio, F. Ciompi, M. Ghafoorian, ... & B. van Ginneken, "A survey on deep learning in medical image analysis," *Medical Image Analysis, 42*, 60-88, 2017. https://doi.org/10.1016/j.media.2017.07.005

[15] V. Priyanka, Kashyap, S. Bhatt, S. J. Bhat, P. Kashyap, & V. Prasad, "MR Parkinsonian index in PSP," Jan. 2017. https://www.researchgate.net/publication/350098663_MR_Parkinsonian_index_in_PSP.

[16] S. Achint, "MRI atlas of normal myelination," 2017. https://www.myelinationmriatlas.com/3-months.html.

[17] C.-Y. Hsu, B. Schneller, M. Ghaffari, A. Alaraj, & A. Linninger, "Medical image processing for fully integrated subject-specific whole brain mesh generation," *Technologies*, vol. 3, pp. 126–141, 2015. doi:10.3390/technologies3020126.

[18] Bernal, J. et al. (2020). "A Framework for Jointly Assessing and Reducing Imaging Artefacts Automatically Using Texture Analysis and Total Variation Optimisation for Improving Perivascular Spaces Quantification in Brain Magnetic Resonance Imaging". In: Papież, B., Namburete, A., Yaqub, M., Noble, J. (eds) Medical Image Understanding and Analysis. *MIUA 2020. Communications in Computer and Information Science, vol 1248. Springer, Cham.* https://doi.org/10.1007/978-3-030-52791-4_14

[19] Bernal, J. et al. (2021). "Selective Motion Artefact Reduction via Radiomics and k-space Reconstruction for Improving Perivascular Space Quantification in Brain Magnetic Resonance Imaging". *In: Papież, B.W., Yaqub, M., Jiao, J., Namburete, A.I.L., Noble, J.A. (eds) Medical Image Understanding and Analysis. MIUA 2021. Lecture Notes in Computer Science, vol 12722. Springer, Cham.* https://doi.org/10.1007/978-3-030-80432-9_12

[20] J. Bernal, M. Valdés-Hernández, J. Escudero, R. Duarte, L. Ballerini, M. E. Bastin, I. J. Deary, M. J. Thrippleton, R. M. Touyz, & J. M. Wardlaw, "Assessment of Perivascular Space Filtering Methods Using a Three-Dimensional Computational Model," *Magnetic Resonance Imaging*, 2022. doi:10.1016/j.mri.2022.07.016.

[21] T. Lindeberg, "Scale-space," in *Scale-Space Theory in Computer Vision*, Springer Berlin Heidelberg, 2009, pp. 1–44. doi:10.1007/978-3-642-02465-4_1.

[22] D. Collins, "Lecture 10: Pyramids and scale space," 2021. https://www.cs.cmu.edu/~./enron/docs/ML/pyramids_and_scale_space.pdf.

[23] E. W. Cheney, & D. R. Kincaid, *Numerical Mathematics and Computing*, 7th ed., Cengage Learning, 2007.

[24] S. Pintea, M. L. Ionescu, D. Enescu, & M. Bogdan, "Perivascular spaces: Imaging modalities and their relationship with cognition," *Frontiers in Human Neuroscience*, vol. 15, 2021. 10.3389/fnhum.2021.754891.

[25] Y. Tominari, & K. Shimizu, "Automatic segmentation of perivascular spaces using deep learning in MR images," *Medical Imaging and Health Informatics*, 2023. 10.1016/j.mihi.2023.101894.

[26] K. Ridgeway, M. R. K. Baig, K. Wang, T. K. Sun, H. Wang, & N. D. Le, "Analyzing perivascular spaces and white matter hyperintensities in cognitively healthy older adults using machine learning techniques," *Nature Scientific Reports*, vol. 13, no. 1, 2023. 10.1038/s41598-023-45294-y.

[27] M. Ismail, A. D. Brown, S. D. O'Connell, & L. P. Collins, "Vesselness filtering method based on deep learning and traditional algorithms for MRA images," *International Journal of Computer Assisted Radiology and Surgery*, 2021. 10.1007/s11548-021-02470-w.

[28] GitHub Documentation: Repository with all the code implemented in this project (open source). [Online]. Available: https://github.com/Riddimental/Frangi-GUI.